

Control of non-Hermitian skin effect by staggered synthetic gauge fields

Tang, Huiyan; Wang, Ziteng; Tang, Liqin; Song, Daohong; Chen, Zhigang; Buljan, Hrvoje

Source / Izvornik: **APL Photonics, 2024, 9**

Journal article, Published version

Rad u časopisu, Objavljena verzija rada (izdavačev PDF)

<https://doi.org/10.1063/5.0196844>

Permanent link / Trajna poveznica: <https://urn.nsk.hr/urn:nbn:hr:217:108007>

Rights / Prava: [Attribution-NonCommercial 4.0 International/Imenovanje-Nekomercijalno 4.0 međunarodna](#)

Download date / Datum preuzimanja: **2025-01-29**



Repository / Repozitorij:

[Repository of the Faculty of Science - University of Zagreb](#)



Control of non-Hermitian skin effect by staggered synthetic gauge fields

Cite as: APL Photon. 9, 056102 (2024); doi: 10.1063/5.0196844

Submitted: 9 January 2024 • Accepted: 15 April 2024 •

Published Online: 1 May 2024



View Online



Export Citation



CrossMark

Huiyan Tang,¹ Ziteng Wang,¹ Liqin Tang,¹ Daohong Song,¹ Zhigang Chen,^{1,a)} and Hrvoje Buljan^{1,2,a)}

AFFILIATIONS

¹TEDA Applied Physics Institute and School of Physics, Nankai University, Tianjin 300457, China

²Department of Physics, Faculty of Science, University of Zagreb, Bijenička Cesta 32, Zagreb 10000, Croatia

^{a)}Authors to whom correspondence should be addressed: zgchen@nankai.edu.cn and hbuljan@phy.hr

ABSTRACT

Synthetic gauge fields introduce an unconventional degree of freedom for studying many fundamental phenomena in different branches of physics. Here, we propose a scheme to use staggered synthetic gauge fields for control of the non-Hermitian skin effect (NHSE). A modified Su–Schrieffer–Heeger model is employed, where two dimer chains with non-reciprocal coupling phases are coupled, exhibiting non-trivial point-gap topology and the NHSE. In contrast to previous studies, the skin modes in our model are solely determined by the coupling phase terms associated with the staggered synthetic gauge fields. By manipulating such gauge fields, we can achieve maneuvering of skin modes as well as the bipolar NHSE. As a typical example, we set up a domain wall by imposing different synthetic gauge fields on two sides of the wall, thereby demonstrating flexible control of the non-Hermitian skin modes at the domain wall. Our scheme opens a new avenue for the creation and manipulation of NHSE by synthetic gauge fields, which may find applications in beam shaping and non-Hermitian topological devices.

© 2024 Author(s). All article content, except where otherwise noted, is licensed under a Creative Commons Attribution (CC BY) license (<https://creativecommons.org/licenses/by/4.0/>). <https://doi.org/10.1063/5.0196844>

INTRODUCTION

Non-Hermitian phenomena are ubiquitous and span across many disciplines.^{1–5} Optical systems have shown to be very suitable to design and explore non-Hermitian phenomena such as parity-time (PT) symmetry.^{6–8} The presence of non-trivial topology in non-Hermitian systems^{9–18} gives rise to topological phenomena quite different from that in their Hermitian counterparts, for example, the behavior of eigenstates and eigenvalues close to exceptional points.^{3,5} Perhaps, one of the most iconic features of the non-Hermitian systems is the non-Hermitian skin effect (NHSE),^{19–37} where a surge of eigenstates piles up toward the boundary of a non-Hermitian system under an open boundary condition (OBC), implying the breakdown of the traditional bulk-boundary correspondence. Remarkably, it is found that the topology associated with the NHSE originates from the point gap of the complex energy spectrum under a periodic boundary condition (PBC), manifested by a non-zero winding number.^{21,22}

Because non-Hermitian systems possess complex energy spectrum, some concepts related to Hermitian bands and gaps are not

applicable. Non-Hermitian systems have two different types of band gaps: point gaps and line gaps.^{4,23} A point gap occurs when the complex-energy bands do not cross a particular point in the complex energy spectrum, and when crossing this point corresponds to a gap-closing transition. On the other hand, when complex energy bands can be separated by a line that does not intersect with any of the bands, a line gap occurs (e.g., see Fig. 5 in Ref. 4). The emergence of point-gap topology implies that the energy spectrum under the PBC forms a loop in the complex plane, with the associated wavevector k being real, indicating extended eigenstates. In contrast, the energy spectrum under the OBC does not overlap with the spectrum under the PBC; the associated wavevector k is complex, corresponding to localized eigenstates better known as the NHSE.

The concept of synthetic gauge fields^{38–43} was introduced in the realm of photonics and ultracold atomic gases over a decade ago, motivated by realizing artificial systems that can mimic the behavior of electrons moving in crystals under the influence of magnetic fields. A typical example is to use such systems for the study of fundamental phenomena that would otherwise occur solely in condensed matter systems, such as the quantum Hall effect. Recent

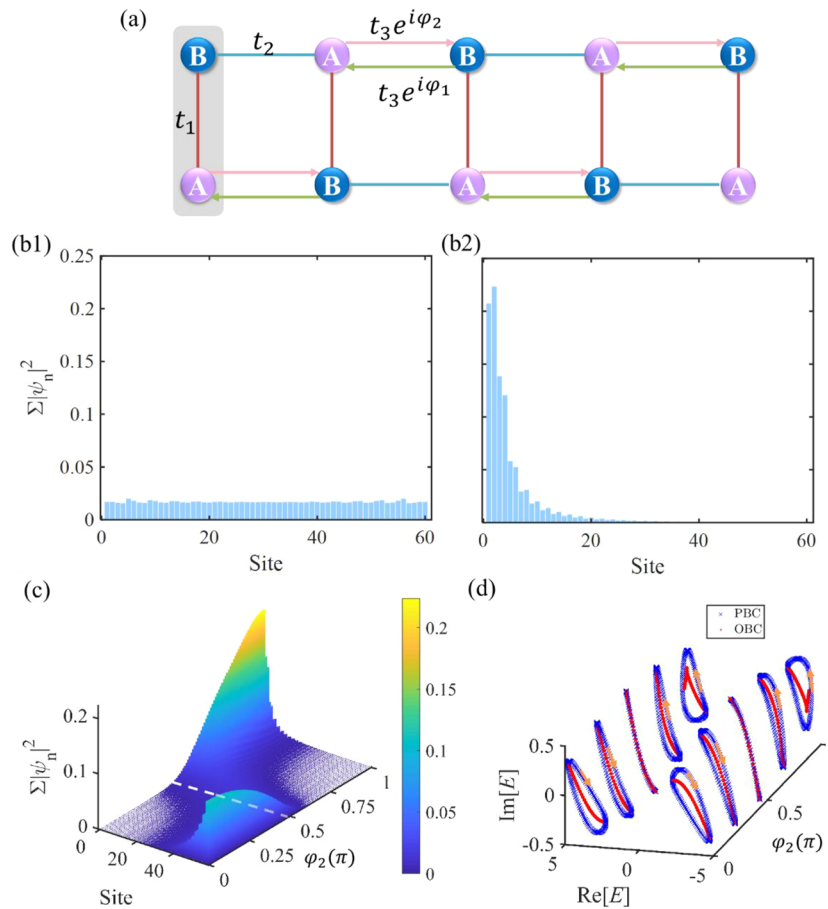


FIG. 1. The modified SSH model and the NHSE. (a) Schematic illustration of a modified SSH lattice. Parameters t_1 and t_2 are reciprocal coupling strengths and $t_3 e^{i\phi_{1,2}}$ are couplings with non-reciprocal phases denoted by ϕ_1 and ϕ_2 . (b1) and (b2) Profiles of eigenmodes under an OBC with $\phi_2 = \pi$ for (b1) $t_1 = 0$ and (b2) $t_1 = 3.5$. (c) Eigenmode distribution with the synthetic gauge field phase ϕ_2 changing from 0 to π . The white dotted line denotes the extended eigenmode, where switching of non-Hermitian skin modes from the right to the left boundary occurs. (d) Complex energy spectra with synthetic gauge fields of the model under the PBC (blue crosses) and the OBC (red dots), with the same parameters as in (c). Orange arrows denote the winding direction of the complex energy spectrum with respect to a reference eigenvalue. Parameters are $t_2 = 1$, $t_3 = 0.5$, $N = 60$, $\phi_1 = \pi/2$, and $t_1 = 3.5$ for (c) and (d).

studies have shown that synthetic gauge fields provide a new degree of freedom to manipulate the NHSE in non-Hermitian systems.^{44–47} Previous achievements include the enhancement of second-order NHSE,³⁷ control of the NHSE via synthetic flux,^{45,46} and the possibility to implement topologically non-trivial non-Hermitian phases via gauge fields.⁴⁷ Most of those studies are focused on the model with a uniform synthetic gauge field and onsite gain and loss to explore topological properties. For example, using a generalized Su–Schrieffer–Heeger (SSH) model^{48–50} with anti-PT-symmetric onsite potentials (gain and loss), one can readily control the NHSE by a uniform synthetic gauge field,⁴⁶ which brings a non-zero effective external magnetic flux through the whole system. One may wonder if the NHSE can be achieved and controlled even without a net external magnetic flux, e.g., by a “staggered” gauge field (which implies an opposite flux in adjacent unit cells but a zero overall

flux through the system). Although it has been proposed that synthetic gauge fields can steer non-Hermitian skin modes in optical ring resonators⁴⁵ and can achieve dynamical control of topologically protected states,⁵¹ to the best of our knowledge, the NHSE has thus far not been realized by using non-reciprocal coupling phases in any system, which provides the motivation for this work.

In this article, we propose a simple yet efficient scheme to achieve and control the NHSE by employing a staggered synthetic gauge field. Inspired by a similar model introduced by Li *et al.*³³ utilizing non-reciprocal coupling magnitudes, here, we focus on the non-reciprocal coupling phases. In particular, we tinker with non-reciprocal coupling phases to ascertain whether staggered gauge fields can be used to manipulate the NHSE. To this end, we consider a pair of coupled non-Hermitian SSH lattices, each of which alone does not feature the NHSE (they have trivial point-gap

topology), as illustrated in Fig. 1. By introducing reciprocal couplings between these two trivial lattices, we demonstrate that the entire (coupled) system exhibits non-trivial point-gap topology and the NHSE mediated by the staggered synthetic gauge field. Such a synthetic gauge field can be fine-tuned to achieve flexible control of the NHSE, illustrated with an example in which a domain wall is created by imposing different gauge fields on the two sides of the wall. Our work offers a new way of exploiting synthetic gauge fields to control non-Hermitian topology and associated NHSE. For practical

implementation, it may be beneficial to achieve tunable NHSE without overall external magnetic flux or onsite gain and loss.

RESULTS

We consider a modified SSH model with non-reciprocal coupling phases depicted in Fig. 1(a). The non-Hermitian Hamiltonian of the model reads

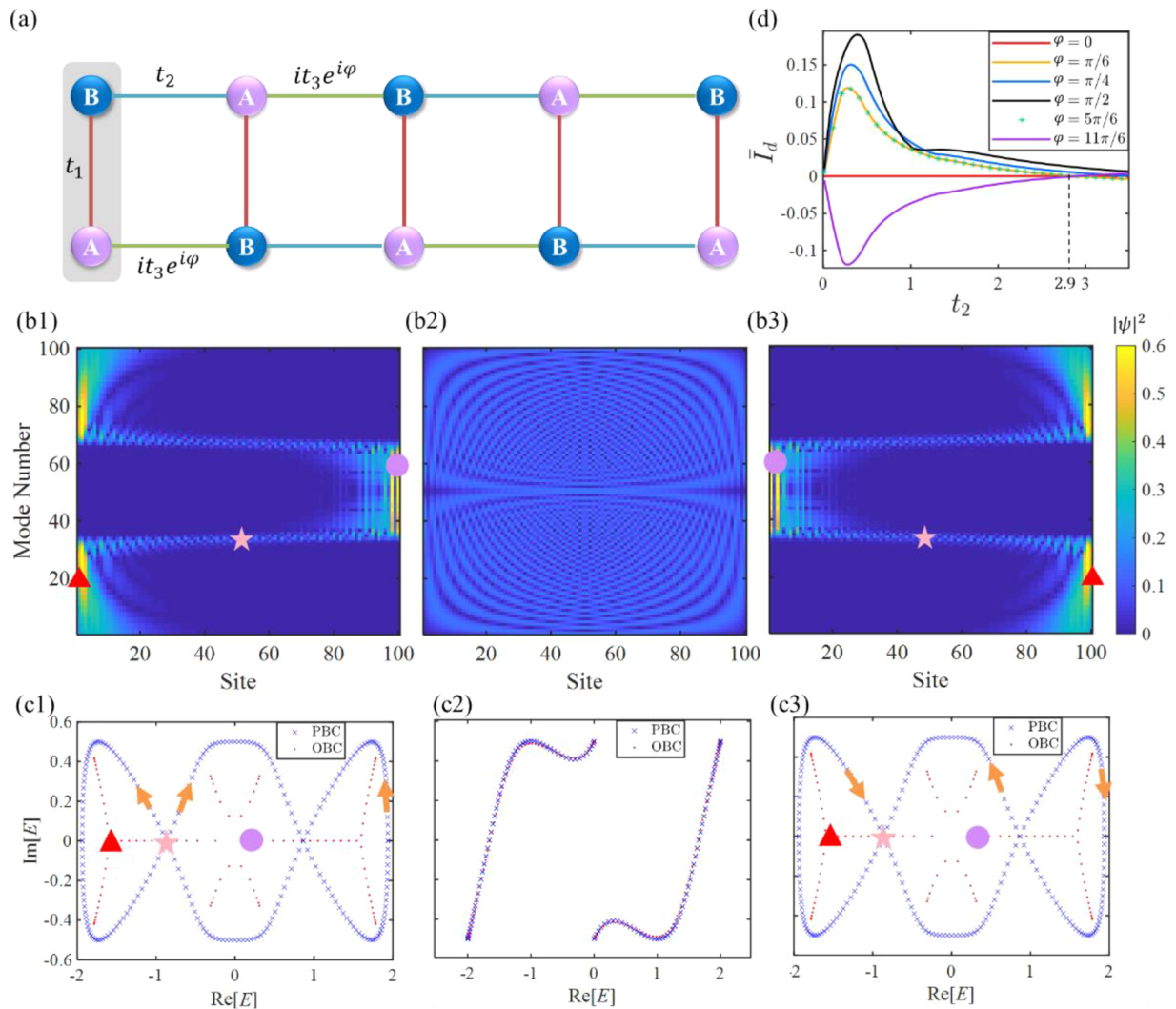


FIG. 2. The modified SSH model and the bipolar NHSE. (a) The equivalent ladder-like lattice of the modified SSH model with staggered synthetic gauge fields. Parameters t_1 and t_2 are real couplings, and $it_3 e^{i\phi}$ is a complex coupling. (b1-b3) Profiles of the eigenmodes of the modified SSH model with the OBC plotted as a function of the lattice site number for (b1) $\phi = -\pi/2$, (b2) $\phi = 0$, and (b3) $\phi = \pi/2$. (c1-c3) Complex energy spectra of the model under the PBC (blue crosses) and the OBC (red dots), with the same parameters corresponding to (b1)–(b3), respectively. Orange arrows denote the winding direction of the complex energy spectrum under the PBC. The triangle and circle in (c1) and (c3) correspond to two representative eigenvalues under the OBC with different winding directions, and the distribution of their eigenmodes is marked in (b1) and (b3). The stars represent Bloch points associated with extended states. (d) The DIPR of the skin modes for different values of ϕ . We plot I_d as a function of the intercell coupling t_2 . The other parameters are chosen to be $t_1 = 1$, $t_2 = 1$, $t_3 = 0.5$, and $N = 100$.

$$H(k) = \begin{pmatrix} 0 & t_1 + t_2 e^{-ik} + t_3 e^{i\varphi_1} e^{ik} \\ t_1 + t_2 e^{ik} + t_3 e^{i\varphi_2} e^{-ik} & 0 \end{pmatrix}, \quad (1)$$

where k is the Bloch momentum, φ_1 and φ_2 denote the non-reciprocal coupling phase terms, and t_i ($i = 1, 2, 3$) are the real magnitudes of the coupling. When $t_1 = 0$, the model is reduced to two decoupled SSH chains. In this case, each of the one-dimensional (1D) SSH models is in a trivial phase regarding point-gap topology [Fig. 1(b1)] because the magnitude of the couplings in each 1D model (t_2 and t_3) is reciprocal. However, when the two SSH chains are coupled ($t_1 \neq 0$), the entire system can exhibit non-trivial point-gap topology with emergence of NHSE [Fig. 1(b2)].

To characterize the NHSE mediated by non-trivial point-gap topology, we evaluate the spectral winding number defined as²¹

$$w(E) = \int_0^{2\pi} \frac{dk}{2\pi i} \frac{d}{dk} \log \det (H(k) - E), \quad (2)$$

where w is the winding number for the eigenvalues of the Hamiltonian with the PBC around a prescribed point E in the complex plane. When E is an eigenvalue of the Hamiltonian with the OBC, a non-zero value of w implies the corresponding eigenstate is localized (NHSE). The sign of w indicates the skin direction, i.e., for a negative (positive) winding number, the skin modes are on the right (left) edge.²⁵ Negative (positive) w corresponds to the clockwise (anticlockwise) winding around E .

We illustrate this in an example in Fig. 1(c): if we keep phase φ_1 fixed, the skin direction of the eigenmodes abruptly changes at a given value of φ_2 , reflecting a topological phase transition from $w = -1$ to $w = 1$. The corresponding complex energy spectra of the PBC and OBC Hamiltonians are shown in Fig. 1(d). By calculating the spectral winding number of Hamiltonian in Eq. (1), we find that the system is topologically non-trivial when $\cos \varphi_1 \neq \cos \varphi_2$. In the non-trivial regime, the PBC energy spectra exhibit a closed curve inside of which there are all the OBC eigenvalues, leading to a non-zero winding number and the existence of the NHSE. This is a typical signature of the NHSE: the eigenvalues for the OBC and the PBC considerably differ. The topological phase transition occurs at $\cos \varphi_1 = \cos \varphi_2$, where the eigenvalues under PBC and OBC coincide, corresponding to a trivial phase containing only extended eigenmodes [see Fig. 1(c)].

Let us now discuss a particular case when the phases φ_1 and φ_2 are related as follows: $\varphi_1 = \pi/2 + \varphi$, $\varphi_2 = \pi/2 - \varphi$, such that we have only a single-phase parameter φ . The model is equivalent to a ladder-like lattice with sites A and B , which hosts real couplings t_1 and t_2 , imaginary couplings it_3 , with a circulation of phase φ in plaquettes corresponding to a staggered synthetic gauge field [Fig. 2(a)]. In the tight-binding approximation, the Hamiltonian of the model in real space reads

$$H_R = \sum_x \left[t_1 \left(\hat{a}_x^\dagger \hat{b}_x + \hat{b}_x^\dagger \hat{a}_x \right) + it_3 \left(e^{i\varphi} \hat{a}_x^\dagger \hat{b}_{x+1} + e^{-i\varphi} \hat{b}_x^\dagger \hat{a}_{x-1} \right) + t_2 \left(\hat{a}_x^\dagger \hat{b}_{x-1} + \hat{b}_x^\dagger \hat{a}_{x+1} \right) \right], \quad (3)$$

where $\hat{a}_x^\dagger (a_x)$ and $\hat{b}_x^\dagger (b_x)$ are, respectively, the creation (annihilation) operators for the sublattice sites A and B on the x th unit cell, respectively. Apart from the conventional NHSE, the model also

exhibits a clear signature of the so-called bipolar NHSE (BNHSE)²⁴ when the eigenmodes collapse to both edges of the lattice.

As the synthetic gauge field parameter φ is varied, the BNHSE is also varied in a controlled fashion. In Figs. 2(b1)–2(c3), we show that by varying φ , we can change the topological phases and the features of the NHSE. The topological phase transition occurs at $\varphi = 0$ [Figs. 2(b2) and 2(c2)]. We use three symbols (star, triangle, and circle) to denote three representative eigenmodes under OBC [Figs. 2(b1), 2(b3), 2(c1), and 2(c3)]. After altering φ from $-\pi/2$ to $\pi/2$, the winding direction (represented by the yellow arrows) is reversed, which moves the skin mode (triangle and circle) from one edge to the other edge. In addition to the localized skin modes, the model has extended eigenmodes marked by stars, which belong to both the PBC and OBC spectra, dubbed the Bloch points.²⁴ It is worth noting that such mode maneuvering involves all skin modes in this process.

Let us evaluate the proportion of the left and right skin modes in the BNHSE as a function of t_2 with different synthetic gauge field phases φ . To quantify the relative proportion of left and right skin modes, we consider the average directional inverse participation ratios (dIPR), defined as³³

$$\bar{I}_d = \frac{1}{2L} \sum_{n=1}^N \sum_{x=1}^L \frac{[x - (L+1)/2] \left(|\psi_{x,n}^A|^4 + |\psi_{x,n}^B|^4 \right)}{(L-1)/2}, \quad (4)$$

with $\psi_{x,n}^s$ being the wave amplitude of the n th normalized eigenmode at site x of sublattice s . N and L are the numbers of the lattice sites and the unit cells, respectively. The dIPR reveals the difference between the distribution of the skin modes on the two edges of the system, i.e., a negative (positive) \bar{I}_d implies that there are more (less) left skin modes in the system than the right ones. As shown in Fig. 2(d), both φ and t_2 influence the spatial distribution of eigenstates quantified by the dIPR. For example, when $\varphi = \pi/6$, the skin modes tend to be localized at the right side for most values of t_2 in the shown interval; above the value $t_2 \simeq 2.9$, the left skin modes become dominant. For $\varphi = 11\pi/6$, most skin modes are localized on the left for $t_2 < 2.9$, and on the right otherwise. The dependence of dIPR on φ is determined by the value of $\sin \varphi$: the magnitude of dIPR reaches a maximum at $\varphi = \pm\pi/2$, whereas for a given value of t_2 , the sign of $\sin \varphi$ determines whether most modes are distributed at the left or the right edge. This allows us to control the proportion of the left and right skin modes by adjusting the synthetic gauge fields. By reversing φ , one can switch between the left skin modes and the right skin modes. The upshot of these results is that a reasonable set of parameters (coupling strength and synthetic gauge field phase) may be chosen for controlling the distribution of left (right) modes.

Next, we discuss how to manipulate wave propagation in our system. For this purpose, we apply a single-site excitation and manipulate the synthetic gauge field over time. Figure 3(b) illustrates numerical results for wave propagation in the lattice shown in Fig. 3(a), whereas Figs. 3(c) and 3(d) show numerical results for wave propagation in the lattice shown in Fig. 2(a), corresponding to the NHSE for $t_1 = 3.5$ [Fig. 3(c)] and to the BNHSE for $t_1 = 1$ [Fig. 3(d)]. The time dependence of the phases is shown in the adjacent panels. The results are obtained by solving $d\psi(t)/dt = iH_R(t)\psi(t)$ with the Runge–Kutta method, where the real space Hamiltonian $H_R(t)$ is time-dependent since φ changes with time. In Fig. 3(c), corresponding to the NHSE, we show that the sign of

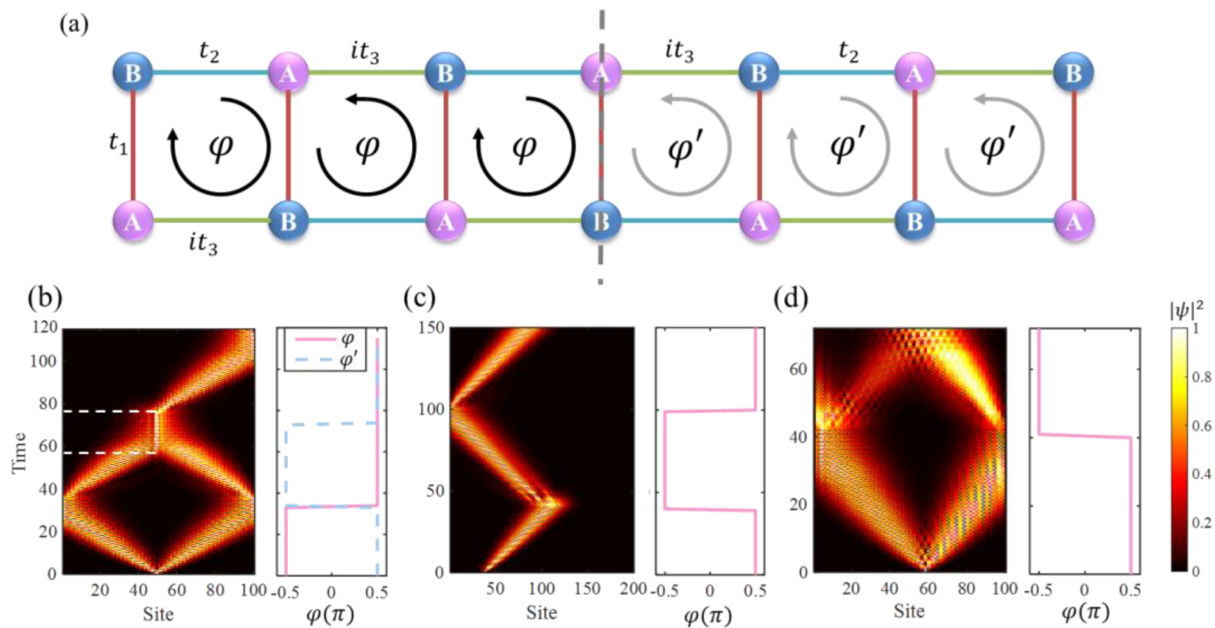


FIG. 3. Domain wall construction and manipulation of the beam dynamics via synthetic gauge fields. (a) A ladder-like lattice with a domain wall (marked by a vertical dashed line) formed by two coupled SSH chains with different staggered phases φ and φ' . (b) Dynamical manipulation of light field evolution in the domain wall model, where the right panel shows the time-dependent phases φ and φ' . Due to the change of the synthetic gauged field phases, the model can be used to achieve beam coalescence (in the range of $60 < t < 80$), beam separation (at $t = 0$), and funneling toward one edge (at $t = 80$). (c) and (d) Examples of dynamical light field manipulation in the modified SSH model with (c) NHSE and (d) BNHSE. The parameters used in the calculation are $t_2 = 1, t_3 = 0.5$, and $t_1 = 3.5$ for (b) and (c), and $t_1 = 1$ for (d).

φ determines whether light is pumped to the left or to the right edge. Thus, by manipulating φ , the “funneling” direction of the modes can be regulated on demand. Interestingly, by employing the BNHSE [Fig. 3(d)], one can achieve mode separation and coalescence by appropriately manipulating the synthetic gauge field phase φ [Fig. 3(d)].

To further demonstrate other possibilities of wave manipulation, we construct a domain wall by imposing different synthetic gauge fields on the two sides of the wall, as shown in Fig. 3(a). The domain wall is formed by employing the model in Eq. (3) and by setting the same coupling strengths but different synthetic gauge field phases (φ and φ') on the two sides of the wall, resulting in the localized skin modes at the wall. In this domain wall construction, the synthetic gauged field can also be varied in time. In Fig. 3(b), we illustrate dynamics where $\varphi = -\pi/2, \varphi' = \pi/2$ for $0 \leq t \leq 35$, $\varphi = \pi/2, \varphi' = -\pi/2$ for $35 < t \leq 75$, and $\varphi = \pi/2, \varphi' = \pi/2$ for $75 < t \leq 115$. We observe rich beam dynamics including beam separation, coalescence, and funneling to one edge. By controlling the position of the domain wall, we can effectively “route” the energy of the beam to any place in the ladder.

DISCUSSION

As we have already mentioned, our model was inspired by the Li, Teo, Mu, and Gong model (LTGM) model,³³ which utilizes non-reciprocal coupling magnitudes in the ladder lattice geometry to obtain the NHSE. Thus, it is worth exploring the connections and differences between our model and the LTGM model. We first note that our model [Fig. 1(a)] cannot be transformed

into the form of the LTGM model via the standard gauge transformations that preserve the flux acquired as a quantum particle (or a wave) goes around one plaquette of the ladder. Flux differs as one goes around the plaquette in a clockwise or counter-clockwise direction (non-Hermitian feature), and it corresponds to (two) values of the synthetic magnetic field flux through one plaquette, which should be gauge-independent quantity. Next, we consider a unitary transformation equivalent to Eq. (23) in Ref. 4. This unitary transformation can cast our model into a model with reciprocal coupling phases, featuring onsite gain and loss. One may argue that the latter Hamiltonian is easier to experimentally implement than our model in Fig. 1, and we do not claim the contrary. However, such a unitary transformation may change the synthetic magnetic flux through plaquettes, leading to a different model from the point of view of synthetic magnetic fields. We emphasize that the purpose of this paper is to explore the possibility of attaining the NHSE with staggered synthetic magnetic fields and non-reciprocal coupling phases.

To this end, let us discuss a possible experimental implementation of our model. The two key ingredients are to construct (i) imaginary coupling between lattice sites supplemented with (ii) an additional synthetic phase, as shown in Fig. 2(a). Both of these ingredients have been addressed before. It was demonstrated that an auxiliary lossy site (in between two sites that we wish to couple) can facilitate imaginary coupling.⁵² On the other hand, synthetic gauge fields have been implemented in versatile platforms,^{38–43} which yields the second ingredient for the desired coupling. An efficient implementation of both ingredients simultaneously is not a trivial

task. The most promising platforms include ring resonators³⁹ and time-multiplexed fiber networks;⁵³ the latter treat time as a new synthetic dimension to generate the coupled lattices.

On a more technical side, components such as beam splitters and intensity modulators are commonly used to induce non-reciprocal coupling strengths in photonic platforms.²⁹ In addition, synthetic phonons have been used to enable non-reciprocal coupling in resonator networks.⁵⁴ However, these components inevitably introduce internal losses that affect the efficiency of a given integrated device. By using phase modulators to manipulate the coupling phases, an alternative approach emerges for the design of non-Hermitian devices, potentially overcoming the limitations of present devices.

CONCLUSION

In summary, we have proposed an approach for achieving and controlling the NHSE by synthetic gauge fields. We have investigated the NHSE in a modified SSH model in which the NHSE arises from a staggered synthetic gauge field without the need for commonly used non-reciprocal coupling strengths or onsite gain and loss. We have demonstrated that our scheme can also support the BNHSE, which is flexibly controlled by adjusting the synthetic gauge field. As a typical example of dynamic manipulation of the NHSE, we have further constructed a domain wall that can be used for effective control of light through mode separation, coalescence, and funneling toward one boundary during propagation. Our work provides an additional route for realizing and controlling non-Hermitian topological systems by synthetic gauge fields, which may find applications in designing non-Hermitian topological devices.

ACKNOWLEDGMENTS

This research was supported by the National Key R&D Program of China (Grant No. 2022YFA1404800), the National Natural Science Foundation of China (Grant Nos. 12134006, 12274242, and 12374309), the project “Implementation of cutting-edge research and its applications as part of the QuantiXLie Center of Excellence,” European Union, European Regional Development Fund, the Natural Science Foundation of Tianjin (Grant Nos. 21JCYBJC00060 and 21JCQJC00050), and the 111 Project (Grant No. B23045) in China.

AUTHOR DECLARATIONS

Conflict of Interest

The authors have no conflicts to disclose.

Author Contributions

Huiyan Tang: Conceptualization (equal); Formal analysis (equal); Investigation (equal); Writing – original draft (equal). **Ziteng Wang:** Conceptualization (equal); Formal analysis (equal); Investigation (equal); Writing – review & editing (equal). **Liqin Tang:** Project administration (equal); Supervision (equal); Writing – review & editing (equal). **Daohong Song:** Project administration (equal); Supervision (equal); Writing – review & editing (equal). **Zhigang**

Chen: Funding acquisition (lead); Project administration (equal); Supervision (equal); Writing – review & editing (equal). **Hrvoje Buljan:** Funding acquisition (equal); Investigation (equal); Supervision (equal); Writing – review & editing (equal).

DATA AVAILABILITY

The data that support the findings of this study are available from the corresponding authors upon reasonable request.

REFERENCES

- C. M. Bender, “Making sense of non-Hermitian Hamiltonians,” *Rep. Prog. Phys.* **70**, 947–1018 (2007).
- N. Moiseyev, *Non-Hermitian Quantum Mechanics* (Cambridge University Press, 2011).
- R. El-Ganainy, K. G. Makris, M. Khajavikhan, Z. H. Musslimani, S. Rotter, and D. N. Christodoulides, “Non-Hermitian physics and PT symmetry,” *Nat. Phys.* **14**, 11–19 (2018).
- E. J. Bergholtz, J. C. Budich, and F. K. Kunst, “Exceptional topology of non-Hermitian systems,” *Rev. Mod. Phys.* **93**, 015005 (2021).
- M. A. Miri and A. Alu, “Exceptional points in optics and photonics,” *Science* **363**, eaar7709 (2019).
- K. G. Makris, R. El-Ganainy, D. N. Christodoulides, and Z. H. Musslimani, “Beam dynamics in PT symmetric optical lattices,” *Phys. Rev. Lett.* **100**, 103904 (2008).
- A. Guo, G. J. Salamo, D. Duchesne, R. Morandotti, M. Volatier-Ravat, V. Aimez, G. A. Siviloglou, and D. N. Christodoulides, “Observation of PT-symmetry breaking in complex optical potentials,” *Phys. Rev. Lett.* **103**, 093902 (2009).
- C. E. Ruter, K. G. Makris, R. El-Ganainy, D. N. Christodoulides, M. Segev, and D. Kip, “Observation of parity-time symmetry in optics,” *Nat. Phys.* **6**, 192–195 (2010).
- S. Weimann, M. Kremer, Y. Plotnik, Y. Lumer, S. Nolte, K. G. Makris, M. Segev, M. C. Rechtsman, and A. Szameit, “Topologically protected bound states in photonic parity-time-symmetric crystals,” *Nat. Mater.* **16**, 433–438 (2017).
- W. Song, W. Sun, C. Chen, Q. Song, S. Xiao, S. Zhu, and T. Li, “Breakup and recovery of topological zero modes in finite non-Hermitian optical lattices,” *Phys. Rev. Lett.* **123**, 165701 (2019).
- H. Zhao, X. D. Qiao, T. W. Wu, B. Midya, S. Longhi, and L. Feng, “Non-Hermitian topological light steering,” *Science* **365**, 1163–1166 (2019).
- A. Cerjan, S. Huang, M. Wang, K. P. Chen, Y. Chong, and M. C. Rechtsman, “Experimental realization of a Weyl exceptional ring,” *Nat. Photonics* **13**, 623–628 (2019).
- K. Wang, A. Dutt, K. Y. Yang, C. C. Wojcik, J. Vuckovic, and S. Fan, “Generating arbitrary topological windings of a non-Hermitian band,” *Science* **371**, 1240–1245 (2021).
- S. Xia, D. Kaltsas, D. Song, I. Komis, J. Xu, A. Szameit, H. Buljan, K. G. Makris, and Z. Chen, “Nonlinear tuning of PT symmetry and non-Hermitian topological states,” *Science* **372**, 72–76 (2021).
- J. Liu, Z. Li, Z. Chen, W. Tang, A. Chen, B. Liang, G. Ma, and J. Cheng, “Experimental realization of Weyl exceptional rings in a synthetic three-dimensional non-Hermitian phononic crystal,” *Phys. Rev. Lett.* **129**, 084301 (2022).
- L. Xiao, T. Deng, K. Wang, G. Zhu, Z. Wang, W. Yi, and P. Xue, “Non-Hermitian bulk–boundary correspondence in quantum dynamics,” *Nat. Phys.* **16**, 761–766 (2020).
- T. Helbig, T. Hofmann, S. Imhof, M. Abdelghany, T. Kiessling, L. W. Molenkamp, C. H. Lee, A. Szameit, M. Greiter, and R. Thomale, “Generalized bulk–boundary correspondence in non-Hermitian topoelectrical circuits,” *Nat. Phys.* **16**, 747–750 (2020).
- A. Ghatak, M. Brandenbourger, J. van Wezel, and C. Coulais, “Observation of non-Hermitian topology and its bulk-edge correspondence in an active

- mechanical metamaterial,” *Proc. Natl. Acad. Sci. U. S. A.* **117**, 29561–29568 (2020).
- ¹⁹S. Yao and Z. Wang, “Edge states and topological invariants of non-Hermitian systems,” *Phys. Rev. Lett.* **121**, 086803 (2018).
- ²⁰T. E. Lee, “Anomalous edge state in a non-Hermitian lattice,” *Phys. Rev. Lett.* **116**, 133903 (2016).
- ²¹Z. Gong, Y. Ashida, K. Kawabata, K. Takasan, S. Higashikawa, and M. Ueda, “Topological phases of non-Hermitian systems,” *Phys. Rev. X* **8**, 031079 (2018).
- ²²H. Shen, B. Zhen, and L. Fu, “Topological band theory for non-Hermitian Hamiltonians,” *Phys. Rev. Lett.* **120**, 146402 (2018).
- ²³K. Kawabata, K. Shiozaki, M. Ueda, and M. Sato, “Symmetry and topology in non-Hermitian physics,” *Phys. Rev. X* **9**, 041015 (2019).
- ²⁴F. Song, S. Yao, and Z. Wang, “Non-Hermitian topological invariants in real space,” *Phys. Rev. Lett.* **123**, 246801 (2019).
- ²⁵K. Zhang, Z. Yang, and C. Fang, “Correspondence between winding numbers and skin modes in non-Hermitian systems,” *Phys. Rev. Lett.* **125**, 126402 (2020).
- ²⁶K. Yokomizo and S. Murakami, “Non-bloch band theory of non-Hermitian systems,” *Phys. Rev. Lett.* **123**, 066404 (2019).
- ²⁷Y. Xiong, “Why does bulk boundary correspondence fail in some non-Hermitian topological models,” *J. Phys. Commun.* **2**, 035043 (2018).
- ²⁸J. Zhong, K. Wang, Y. Park, V. Asadchy, C. C. Wojcik, A. Dutt, and S. Fan, “Nontrivial point-gap topology and non-Hermitian skin effect in photonic crystals,” *Phys. Rev. B* **104**, 125416 (2021).
- ²⁹S. Weidemann, M. Kremer, T. Helbig, T. Hofmann, A. Stegmaier, M. Greiter, R. Thomale, and A. Szameit, “Topological funneling of light,” *Science* **368**, 311–314 (2020).
- ³⁰W. Wang, X. Wang, and G. Ma, “Non-Hermitian morphing of topological modes,” *Nature* **608**, 50–55 (2022).
- ³¹S. Weidemann, M. Kremer, S. Longhi, and A. Szameit, “Topological triple phase transition in non-Hermitian Floquet quasicrystals,” *Nature* **601**, 354–359 (2022).
- ³²X. Zhang, T. Zhang, M. Lu, and Y. Chen, “A review on non-Hermitian skin effect,” *Adv. Phys.: X* **7**, 2109431 (2022).
- ³³L. Li, W. Teo, S. Mu, and J. Gong, “Direction reversal of non-Hermitian skin effect via coherent coupling,” *Phys. Rev. B* **106**, 085427 (2022).
- ³⁴T. Liu, Y. Zhang, Q. Ai, Z. Gong, K. Kawabata, M. Ueda, and F. Nori, “Second-order topological phases in non-Hermitian systems,” *Phys. Rev. Lett.* **122**, 076801 (2019).
- ³⁵X. Zhang, Y. Tian, J. Jiang, M. Lu, and Y. Chen, “Observation of higher-order non-Hermitian skin effect,” *Nat. Commun.* **12**, 5377 (2021).
- ³⁶K. Zhang, Z. Yang, and C. Fang, “Universal non-Hermitian skin effect in two and higher dimensions,” *Nat. Commun.* **13**, 2496 (2022).
- ³⁷C. Li, B. Trauzettel, T. Neupert, and S. Zhang, “Enhancement of second-order non-Hermitian skin effect by magnetic fields,” *Phys. Rev. Lett.* **131**, 116601 (2023).
- ³⁸M. Rechtsman, J. Zeuner, Y. Plotnik, Y. Lumer, M. Segev, A. Szameit, S. Nolte, M. Segev, and A. Szameit, “Photonic Floquet topological insulators,” *Nature* **496**, 196–200 (2013).
- ³⁹M. Hafezi, S. Mittal, J. Fan, A. Migdall, and J. Taylor, “Imaging topological edge states in silicon photonics,” *Nat. Photonics* **7**, 1001–1005 (2013).
- ⁴⁰R. O. Umucalilar and I. Carusotto, “Artificial gauge field for photons in coupled cavity arrays,” *Phys. Rev. A* **84**, 043804 (2011).
- ⁴¹K. Fang, Z. Yu, and S. Fan, “Realizing effective magnetic field for photons by controlling the phase of dynamic modulation,” *Nat. Photonics* **6**, 782–787 (2012).
- ⁴²A. Celi, P. Massignan, J. Ruseckas, N. Goldman, I. B. Spielman, G. Juzeliunas, and M. Lewenstein, “Synthetic gauge fields in synthetic dimensions,” *Phys. Rev. Lett.* **112**, 043001 (2014).
- ⁴³Y. Lumer, M. A. Bandres, M. Heinrich, L. J. Maczewsky, H. Herzig-Sheinfux, A. Szameit, and M. Segev, “Light guiding by artificial gauge fields,” *Nat. Photonics* **13**, 339–345 (2019).
- ⁴⁴L. Du, Y. Zhang, and J. Wu, “Controllable unidirectional transport and light trapping using a one-dimensional lattice with non-Hermitian coupling,” *Sci. Rep.* **10**, 1113 (2020).
- ⁴⁵Z. Lin, L. Ding, S. Ke, and X. Li, “Steering non-Hermitian skin modes by synthetic gauge fields in optical ring resonators,” *Opt. Lett.* **46**, 3512–3515 (2021).
- ⁴⁶C. Wu, Z. Yang, J. Tang, N. Liu, and G. Chen, “Flux-controlled skin effect and topological transition in a dissipative two-leg ladder model,” *Phys. Rev. A* **106**, 062206 (2022).
- ⁴⁷W. Rui, Y. Zhao, and Z. Wang, “Making topologically trivial non-Hermitian systems nontrivial via gauge fields,” *Phys. Rev. Lett.* **131**, 176402 (2023).
- ⁴⁸W. P. Su, J. R. Schrieffer, and A. J. Heeger, “Solitons in polyacetylene,” *Phys. Rev. Lett.* **42**, 1698–1701 (1979).
- ⁴⁹N. Malkova, I. Hromada, X. Wang, G. Bryant, and Z. Chen, “Observation of optical Shockley-like surface states in photonic superlattices,” *Opt. Lett.* **34**, 1633–1635 (2009).
- ⁵⁰A. Blanco-Redondo, B. Bell, D. Oren, B. J. Eggleton, and M. Segev, “Topological protection of biphoton states,” *Science* **362**, 568–571 (2018).
- ⁵¹L. Du, J. Wu, M. Artoni, and G. La Rocca, “Phase-dependent topological interface state and spatial adiabatic passage in a generalized Su-Schrieffer-Heeger model,” *Phys. Rev. A* **100**, 012112 (2019).
- ⁵²S. Longhi, “Non-Hermitian bidirectional robust transport,” *Phys. Rev. B* **95**, 014201 (2017).
- ⁵³C. Leefmans, A. Dutt, J. Williams, L. Yuan, M. Parto, F. Nori, S. Fan, and A. Marandi, “Topological dissipation in a time-multiplexed photonic resonator network,” *Nat. Phys.* **18**, 442–449 (2022).
- ⁵⁴C. W. Peterson, S. Kim, J. T. Bernhard, and G. Bahl, “Synthetic phonons enable non-reciprocal coupling to arbitrary resonator networks,” *Sci. Adv.* **4**, eaat0232 (2018).